RESEARCH ARTICLE

Temperature imaging of turbulent dilute spray flames using two-line atomic fluorescence

Paul R. Medwell · Assaad R. Masri ·
Phuong X. Pham · Bassam B. Dally ·
Graham J. Nathan

Abstract This paper reports the first application of non-linear excitation regime two-line atomic fluorescence imaging (NTLAF) of indium to measure temperature in turbulent flames of dilute sprays. Indium chloride is dissolved in acetone fuel which is atomised with an ultrasonic nebuliser and supplied with carrier air into a standard piloted burner. It is found that the indium fluorescence signal is not affected by scattering from the droplets or fuel vapour and that no changes to the optical arrangement used with gaseous flames were required. Notwithstanding the lower temperature thresholds of 800 K imposed by the population of excitation species for the NTLAF method and of 1,200 K imposed by the mechanism of releasing gas-phase indium from its salt, the comparisons of conditional and pseudo-unconditional means with thermocouple measurements performed in a range of turbulent spray flames are quite favourable. The NTLAF signal quality deteriorates on the jet centreline at upstream locations and on the lean side of the flame, the former being largely due to insufficient conversion of indium chloride to indium atoms and the latter potentially due to indium oxidation. Nevertheless, the signal-to-noise ratios obtained in the reaction zone regions are good and the results reveal the expected temperature trends in the turbulent spray flames tested here. Further developments are necessary to resolve the mechanism of indium formation and to broaden the temperature range.

P. R. Medwell (✉) · B. B. Dally · G. J. Nathan
School of Mechanical Engineering, The University of Adelaide,
Adelaide, SA 5005, Australia
e-mail: paul.medwell@adelaide.edu.au

A. R. Masri · P. X. Pham
School of Aerospace, Mechanical and Mechatronic Engineering,
The University of Sydney, Sydney, NSW 2006, Australia

1 Introduction

Diagnostic capabilities in spray flows are gradually evolving but remain limited due to inherent difficulties imposed by the presence of droplets and/or liquid filaments. Dense sprays are extremely hard to probe and techniques such as ballistic imaging (Linne et al. 2005, 2009, 2010) and X-ray radiography (MacPhee et al. 2002; Ramírez et al. 2009; Wang et al. 2006) are just starting to make advances in measuring the spray structure and the mass depletion from the liquid core (Linne 2013). Dilute spray flames are relatively easier but still challenging, particularly with respect to measuring details of the mixing and reactive fields. Laser-induced fluorescence (LIF) techniques were applied to image selected species such as OH, CH_2O, or fuel vapour (Stårner et al. 2005; O'Loughlin and Masri 2011, 2012; Fansler et al. 2009). These measurements, while qualitative, reveal interesting information about the structure and evolution of reaction zones. However, measurements of critical parameters such as mixture fraction and temperature remain elusive. This paper addresses one of these problems by introducing an approach to measure temperature in turbulent dilute spray flames.

Measurement of temperature in flows laden with solid particles or droplets is very difficult. Standard techniques, such as Rayleigh scattering, are no longer applicable due to corruption by Mie scattering. Coherent anti-Stokes Raman spectroscopy (CARS) is a well-established technique for accurate measurements of temperature in flames containing soot (Brackmann et al. 2002; Roy et al. 2010; Kearney et al. 2009; Weikl et al. 2009; Köhler et al. 2011) and more recently in spray flames (Weikl et al. 2006; Engel et al. 2012). Notwithstanding recent developments in CARS (Bohlin et al. 2013; Bohlin and Kliewer 2013), which are

yet to be fully exploited, a key limitation of this technique lies in its ability to provide only single-point measurements rather than more desirable large-scale planar information. Thermometry based on multi-line fluorescence from molecular species such as NO offers capability for two-dimensional imaging, but these methods remain limited to time-averaged measurements (Kronemayer et al. 2005). Two-line thermometry of OH (Stelzner et al. 2013; Devillers et al. 2008; Kostka et al. 2009) offers several advantages, but the relatively narrow range of combustion intermediates in mixture fraction space imposes a limitation for non-premixed flames. Two-line atomic fluorescence (TLAF) techniques can fill this gap, as demonstrated recently through imaging of instantaneous planar temperature fields in turbulent flames containing soot (Chan et al. 2011; Nathan et al. 2012). The objective of this paper is to extend such capabilities to turbulent dilute spray flames.

The operating principle of TLAF is based on the sequential excitation from two lower energy states of an atomic species (Alkemade 1970), typically indium (Omenetto et al. 1972; Haraguchi et al. 1977). A range of detection schemes are possible (Zizak et al. 1984), although the resultant fluorescence is most commonly detected at the opposite wavelength of the excitation process. For convenience, these transitions are referred to as Stokes (410 nm excitation, 450 nm detection) and anti-Stokes (450 nm excitation, 410 nm detection). The technique has been progressively developed (Aldén et al. 1983) to include high-speed measurements (Dec and Keller 1986), measurements in engines (Kaminski et al. 1998), and sooting flames (Engström et al. 2000; Nygren et al. 2001), and with the application of diode lasers (Hult et al. 2005; Burns et al. 2011). The extension of TLAF to the nonlinear excitation regime, so called NTLAF (Medwell et al. 2009), has enabled instantaneous temperature imaging in turbulent non-premixed gaseous flames (Medwell et al. 2013) and flames containing soot (Chan et al. 2011). Two alternative seeding arrangements have been considered: nebulisation of a solvent containing indium chloride and laser ablation of a solid indium rod (Medwell et al. 2013). A range of solvents were considered for the nebulisation seeding approach (Chan et al. 2010). However, for gaseous flames, the inclusion of a liquid stream introduces some physical changes compared with the non-seeded flame. Laser ablation of a solid rod of indium eliminates many of these issues, but introduces new complexities which are yet to be fully resolved (Medwell et al. 2012; Chan et al. (2012). The for case of spray flames, dissolving indium chloride in the fuel stream is most convenient and avoids the need to introduce another stream into the system. It is important to note that, irrespective of the seeding method, the measurement is inherently conditional on two key factors: the temperature of the indium must exceed

800 K to generate sufficient anti-Stokes signal and the indium must be present as neutral atoms in the measurement volume. The release of neutral indium atoms from the seeded material typically requires interaction with the flame front and is also favoured under fuel-rich conditions, since indium is readily oxidised (Medwell et al. 2009); therefore, measurements are only possible in certain regions of the flame (Medwell et al. 2010). It should be noted that although the conversion of indium chloride solution to gas-phase neutral indium atoms is a crucial step for TLAF thermometry, to successfully apply the technique it is not necessary to have a complete understanding of the thermochemical conditions required for the decomposition process and the chemical kinetics.

With spray flames, there is an opportunity to seed the liquid fuel with indium chloride and thus avoid the need for introducing an additional stream as required for turbulent gaseous flames (Medwell et al. 2013). Although the NTLAF technique is generally immune from interferences due to soot scattering, insufficient information is available to determine whether interference from the fuel droplets in spray flames will allow the seeding advantages to be realised. Specifically, the following issues are to be resolved by this study:

- Previous studies using NTLAF in sooting flames have shown that interference from scattering is a limiting factor in the signal-to-noise ratio of the measurement. For example, for an ethylene flame, the interference was 5 % for a soot volume fraction of approximately 1 ppm, rapidly increasing to a 200 % uncertainty in the deduced temperature at the maximum soot volume of 3 ppm (Chan et al. 2011). Hence, it is important to assess the influence of scattering from droplet environments, where scattering is significant.

- The scattering from droplets in the present spray flame can be expected to be very much larger than that from the droplets employed with the nebuliser in previous work (Medwell et al. 2013) because of their much greater size. The Sauter mean diameter (d) of the droplets employed in the current investigation is 37–45 µm, in contrast to the 5-µm-diameter droplets employed in the previous seeding. Since the Mie scattering interference scales with d^2, the interference from the larger spray droplets used in the present system can be expected to be two orders of magnitude stronger per droplet. However, the scattering also depends on the local number density, which is difficult to predict a priori. Hence, it is necessary to verify whether these interferences are significant.

- The number of droplets per unit volume scales with $1/d^3$. Hence, the use of droplets of an order of magnitude larger diameter implies three orders of

magnitude fewer droplets. This, in turn, implies a much less uniform dispersion of the indium into the flame. Hence, the new seeding methodology may be expected to result in a less effective dispersion into the flame and a greater bias in the temperature measurement.

- The bias in the seeding may be augmented by a possible nonlinearity between the rate of release of indium chloride and the rate of evaporation. That is, the evaporation may result in a change of concentration of indium salt before it is released into the gas phase. This is a further possible method of mitigating the effectiveness of seeding, which is too difficult to calculate a priori and requires experimental testing.

- The wetting of liquid on the walls of the nozzle also generates occasional instances of very large droplets being released into the flame, of diameter ~ 1 mm. Importantly, the influence of scattering from such large particles has not been assessed previously.

The aim of the current paper is, therefore, to assess, for the first time, the feasibility of conducting instantaneous single-shot temperature imaging in turbulent spray flames using the NTLAF technique. Importantly, the capabilities of the technique are assessed using the same optical arrangement used in previous studies, without modifications to account for the potential interferences from the droplets. Such temperature measurements, if realised, would lead to significant insight into some important and outstanding aspects of turbulent spray flames.

2 Experimental setup

2.1 Burner details

The piloted burner design adopted in this study, and shown schematically in Fig. 1, is similar to that used previously for investigating processes of auto-ignition (O'Loughlin and Masri 2011) and combustion (Stårner et al. 2005; Gounder et al. 2012) in turbulent dilute sprays. A key feature of the design lies in the simplicity of the flow and the provision of well-controlled boundary conditions to facilitate modelling (Jenny et al. 2012). The droplets are generated upstream by an ultrasonic nebuliser and carried by air along a tube ($D = 7$ mm, length = 196 mm) to the exit plane. Other gases could be used to carry the droplets, but air only is used here. The fuel tube is surrounded by a pilot flame ($D = 24$ mm) that ensures the main flame remains attached to the jet exit plane.

The four flames shown in Fig. 2, with operating conditions shown in Table 1, were selected for investigation. These flames are selected to assess the effects of changing
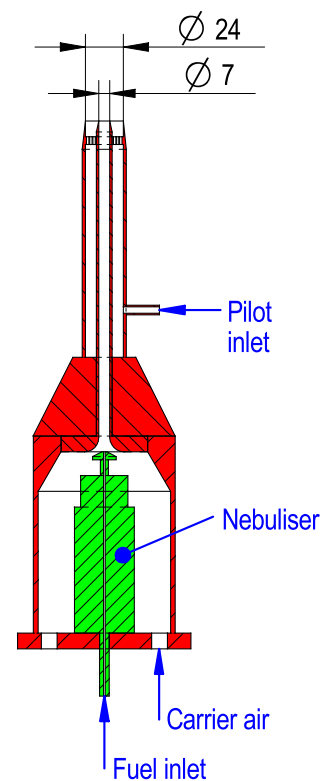

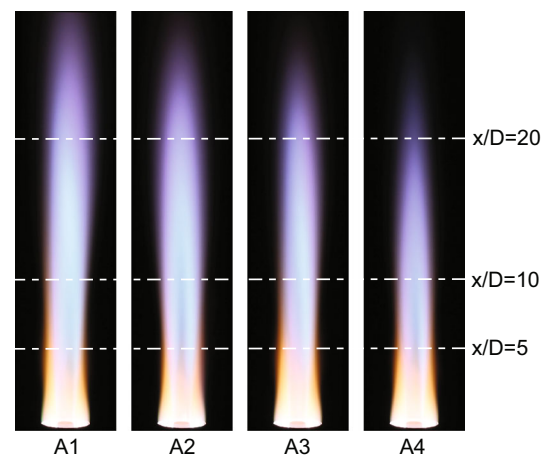Fig. 1 Cross-sectional representation of dilute spray burner

Fig. 2 Photographs of the four flames assessed. Refer to Table 1 for operating conditions. Image height = 200 mm. The internal diameter of the central fuel jet, $D = 7$ mm

the liquid loading for the same air carrier velocity and vice versa. The bulk velocity ratio ($U_{\text{jet}}/U_{\text{b.o.}}$) stated in Table 1 refers to the ratio of the bulk exit velocity to the blow-off limit. Figure 3 shows the location of the flames and blow-off limit. Given the same liquid loading, flames A2 and A4 are closer to blow-off and slightly shorter than their counterparts (flames A1 and A3, respectively), due to the higher jet Reynolds number. Flame A4 is the closest to

Table 1 Acetone spray flames: jet fuel and air flow-rates

Flame	Acetone (g/min)	Air (g/min)	Re_{jet}	Φ_{jet}	$U_{jet}/U_{b.o.}$ (%)
A1	13	100	16,500	1.23	69
A2	13	125	25,000	0.98	87
A3	9.5	100	16,500	0.90	76
A4	9.5	125	25,000	0.72	95

Bulk jet Reynolds number determined from air flow-rate. Equivalence ratio (Φ) does not distinguish between acetone in vapour or liquid phase. U_{jet} is the air jet velocity and $U_{b.o.}$ the air velocity at which blow-off occurs for a given acetone mass flow-rate
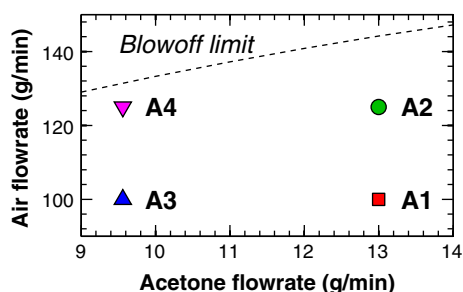
Fig. 3 Blow-off limit and flame conditions (refer to Table 1)

blow-off and hence the shortest. All four flames remain attached to the burner are also free from visible evidence of soot and do not exhibit droplet shedding (the formation of liquid ligaments) from the burner's exit plane. The pilot flame is a stoichiometric mixture of acetylene, hydrogen, and air such that the C/H ratio matches the liquid fuel (acetone). The bulk unburnt pilot velocity is maintained throughout all tests at 1.0 m/s, with a constant heat release from the pilot to all flames: 25 % of the total heat release for flames A1 and A2 decreasing to 20 % for flames A3 and A4.

Some evaporation of the droplets occurs within the main fuel tube, the extent of which depends on the relative flow of acetone and carrier air. In earlier work (Gounder et al. 2012), it was found that $40-75$ % of the liquid may be evaporated by the time it reaches the exit plane of the burner. The Sauter mean diameter on the jet centreline ranges from 37 to 45 microns, and the spray at the burner's exit is found to follow closely the Nukiyama–Tanasawa distribution (Gounder et al. 2012). Extensive details of the in-flow boundary conditions have previously been reported by Gounder (2009). The three measurement locations (x/D = 5, 10 and 20) are also indicated on Fig. 2, where D is the diameter of the central jet. For the purposes of the NTLAF technique, indium chloride is added to the acetone fuel supply at a concentration of 375 mg/L, which is

selected to provide strong LIF signal without excessive use of seed.

2.2 Optical arrangement

Extensive details of the experimental layout for the non-linear excitation regime two-line atomic fluorescence technique may be found in previous publications (Medwell et al. 2009, 2013), and only a brief description is given here. Two Nd:YAG-pumped dye lasers are fired with 100 ns separation, to produce the required 410.18 and 451.13 nm excitation beams, with line widths of 0.4 and $0.3\,\mathrm{cm}^{-1}$, respectively. The two 2 mJ/pulse beams are combined and circularly polarised with the use of a quarter-wave plate. The beams are subsequently directed through a cylindrical telescope lens system to produce a coplanar sheet of $\sim 300\,\mu\mathrm{m}$ thickness. The beams pass through two glass slides to generate diffuse scattering which is detected with a CCD camera through interference filters to provide shot-to-shot corrections of spatial variations in the laser energy profile across the sheet height. No modifications to the optical arrangement used previously for gaseous flames have been made for the current spray flames. This enables a direct assessment of the capability of the technique in the presence of liquid droplets.

3 Results and discussion

3.1 Instantaneous images

To assess the efficacy of the liquid-fuelled seeding approach, Fig. 4 presents representative images of instantaneous indium fluorescence collected at three axial locations in each of the four flames (Table 1). Each image window shows simultaneous Stokes and anti-Stokes indium fluorescence intensity, respectively, on either side of the jet centreline (where the anti-Stokes image has been flipped left–right). Images at different heights are uncorrelated in time, but a constant colour-scaling is adopted throughout all images.

Figure 4 confirms that good fluorescence signals are obtained at these relevant locations in the flames. The signal-to-noise ratios (SNR) of the instantaneous fluorescence images are $\sim 20{:}1$ for Stokes and $\sim 10{:}1$ for anti-Stokes. These are higher than those obtained in previous measurements performed in gaseous turbulent jet flames using the same NTLAF technique with the seeding via indium chloride Medwell et al. (2013). This improvement may be partly due to the higher seeding concentration employed here, where approximately 40 ppm of $InCl_3$ is used in the current spray flames, compared with 25 ppm in
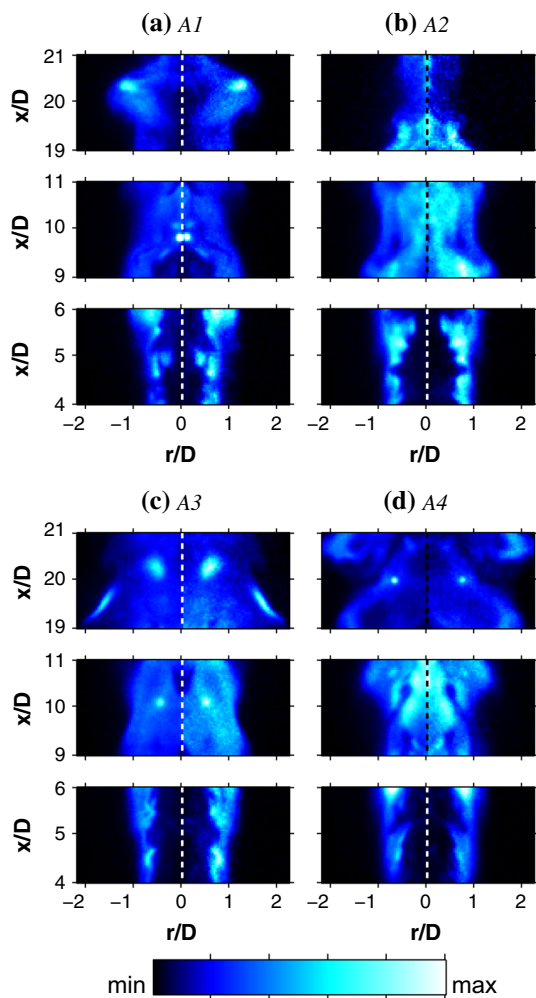
Fig. 4 Selection of instantaneous raw indium fluorescence images for the four flames at various axial (*x/D*) locations. *Left-hand* and *right-hand* side of centreline (*vertical dashed line*) are Stokes and anti-Stokes images, respectively (where anti-Stokes image has been flipped *left–right*). Images at each location are temporally not correlated, and all images have the same colour-scale

gaseous flames (Medwell et al. 2013). It is worth noting, however, that an increase in indium chloride concentration alone does not necessary lead to a commensurate improvement in SNR (Medwell et al. 2009) since the conversion of indium chloride to indium atoms is a key process that remains only vaguely understood and hence in need of further research. Importantly, the concentration of neutral indium atoms is sufficient to yield fluorescence signal, such that the lack of understanding of the fate of indium in the flame does not lead to uncertainty in the NTLAF measurements.

The sample images of Fig. 4 show consistent trends with those expected for gaseous jet flames as well as the spray flames studied here. At $x/D = 4-6$, no fluorescence signal is detected in the potential core of the jets where the temperature is relatively low. Although a significant

proportion of the fuel has evaporated before exiting the pipe, the indium salt must first be transformed into neutral indium atoms, and this has previously only been observed in the vicinity of a local reaction zone (Medwell et al. 2010). This is also evident here where good signals are obtained in the flame zone outside the potential core. In the case where the indium salt is bound in un-evaporated droplets, no fluorescence signal is detected, but this does not skew the results because in these cases, the temperature would be below the lower temperature limit of the technique. Importantly, the images show no significant evidence of interference from either Mie scattering or PAH fluorescence, and this was further confirmed by de-tuning the dye laser wavelength away from the indium excitation transitions. Further downstream, at $x/D = 9-21$, fluorescence is detected across the entire flame, including the centreline, which is also expected for non-premixed or partially premixed flames.

In addition to the four flames presented in Table 1, data were also collected in flames with significant droplet shedding. This is characterised by large ($\gtrsim 1$ mm) droplets and achieved by exceeding the optimal liquid fuel flowrate. The motivation of these additional measurements was to assess the capabilities of the technique at rejecting interferences from the very large droplets. It was found that even under these extreme conditions, the interference from these droplets was less than 2 %. This highlights the robustness of the NTLAF technique to scattering from the droplets encountered in spray flames.

3.2 Indium fluorescence intensity

Figure 5 presents the mean radial profiles of the Stokes and anti-Stokes fluorescence intensity measured at various axial locations in each of the four flames considered here. The same scaling is applied throughout all flames and measurement locations so that the Stokes and anti-Stokes fluorescence is normalised by the maximum value so that a peak relative fluorescence of 100 % is shown. Despite the concentration of indium chloride being maximum closest to the jet exit plane (*viz.* $x/D = 5$), the integrated indium fluorescence signal is shown to peak at $x/D = 10$. This implies that the conversion process of indium chloride to neutral indium atoms has not occurred in the potential core region and requires interaction with the flame front. The low signal along the centreline at $x/D = 5$ is therefore related to the thermochemical conditions and residence time being insufficient to release neutral indium atoms in this region, consistent with the instantaneous images presented in Fig. 4 and discussed in Sect. 3.1. At $x/D = 5$, the influence of the pilot is still significant so that all flames have similar radial profiles and this is clear from Fig. 5. Further downstream, and consistent with images of Fig. 4,
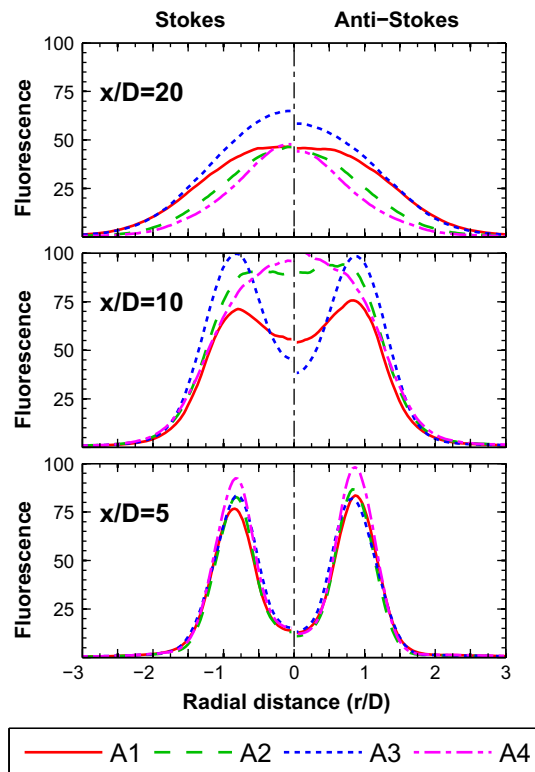
Fig. 5 Mean indium fluorescence intensity radial profiles (arbitrary units) for Stokes and anti-Stokes transitions at various axial x/D locations for the four flames (refer to Table 1)

is that the profiles are broader and fluorescence signals are higher on the centreline. Moreover, different peaks are observed for different flames due to the fact that the influence of the pilot has diminished and finite-rate chemistry comes into effect at these locations. These consistent results confirm the validity of the technique and its potential for providing a measure of temperature in the dilute spray flames as further discussed in the remainder of this paper.

3.3 Instantaneous conditional temperature images

Figure 6 presents the instantaneous temperature images derived from the NTLAF technique, which are conditional based on the conversion of the seeded salt into neutral indium atoms and the temperature being high enough to yield sufficient signal from the anti-Stokes transition. The conditional temperature images in Fig. 6 show both sides of the flame, whereas only the fluorescence images corresponding to the left-hand side of the conditional temperature images are shown in Fig. 4 (noting that the anti-Stokes image has been flipped left-to-right about the centreline in Fig. 4).

The interpixel "noise" in the instantaneous conditional temperature images is 130 K (6 %), an improvement
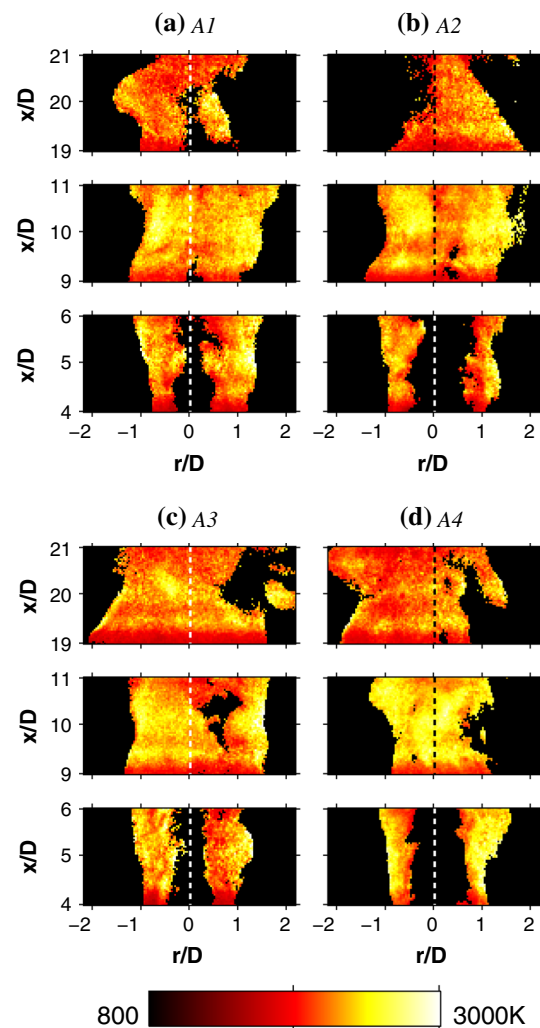

Fig. 6 Selection of instantaneous conditional temperature images for the four flames at various axial (x/D) locations. Images at each x/D are temporally not correlated, and all images have the same constant colour-scale (in Kelvin)

compared with previous seeding approaches (Medwell et al. 2013). In regions with low temperature, the anti-Stokes signal is low and thus leads to unacceptably low SNR. To avoid this, the lower temperature limit imposed in the image processing for these flames is 800 K. Pixels where the anti-Stokes fluorescence is below the intensity corresponding to 800 K are assigned a presumed temperature value of 300 K. Previous studies in turbulent flames (Medwell et al. 2013) have required a higher temperature (fluorescence) threshold, corresponding to 1,200 K. In previous measurements, the SNR of the anti-Stokes fluorescence in the range 800–1,200 K was too low to give meaningful temperature results. Consequently, a threshold was imposed on the anti-Stokes fluorescence data corresponding to a temperature of 1,200 K. In the current measurements, this threshold has been able to be reduced

because of the improved SNR, enabling measurements down to 800 K. The difference in the lower temperature threshold indicates an improvement in the performance of the technique for these spray flames over previous gaseous flames. Further discussion on the threshold temperature is provided in Sect. 3.4.

It can be observed from Fig. 6 that the instantaneous conditional temperature images are mostly uniform in all flames shown here. This is consistent with the broad flame front observed in previous OH-LIF imaging (Masri and Gounder 2010) and implies that evaporation has little, if any, direct influence on the structure of the flame front. Neither the temperature images in Fig. 6 nor the previous OH-LIF images show significant increase or decrease in the region surrounding the droplets. This is consistent with these sprays being dilute so that droplet evaporation is not a rate-limiting factor. Future work may enable further elucidation of this issue.

The uniformity of the conditional temperature images (Fig. 6) somewhat contrasts that seen in the fluorescence images (Fig. 4). For example, in the fluorescence image of flame A1 (Fig. 4a) at $x/D = 20$ a clearly identifiable pocket of strong signal is noted at $r/D \approx 1$ while only minor variations are observed at this location in the corresponding conditional temperature (Fig. 6a). Similar observations may be noted for other pockets of strong indium fluorescence in the other images. These findings suggest that droplets, or other regions of high indium concentration, do not significantly bias the conditional temperature measurements. This is an important result because it highlights the capabilities of the technique to obtain measurements in close proximity to liquid droplets.

3.4 Temperature results

Figure 7 presents the mean and RMS radial conditional temperature profiles measured at three axial locations in four flames. Each profile is determined from a minimum of 600 instantaneous images. As noted above, the temperature measurements are conditional upon the temperature exceeding 800 K and also requires gas-phase indium to be present. This is favoured under fuel-rich conditions. The conditional nature of the measurements and hence, the derived quantities, requires care with analysis and interpretation. The pseudo-unconditional mean was calculated from the mean of all pixels in the temperature image, including those where NTLAF data were not available (either because of low indium concentration or a temperature below 800 K), which are assigned an assumed temperature of 300 K. This pseudo-unconditional average will inevitably underestimate the true unconditional average somewhat (because it cannot resolve any temperature measure below 800 K). It is nevertheless a consistent and
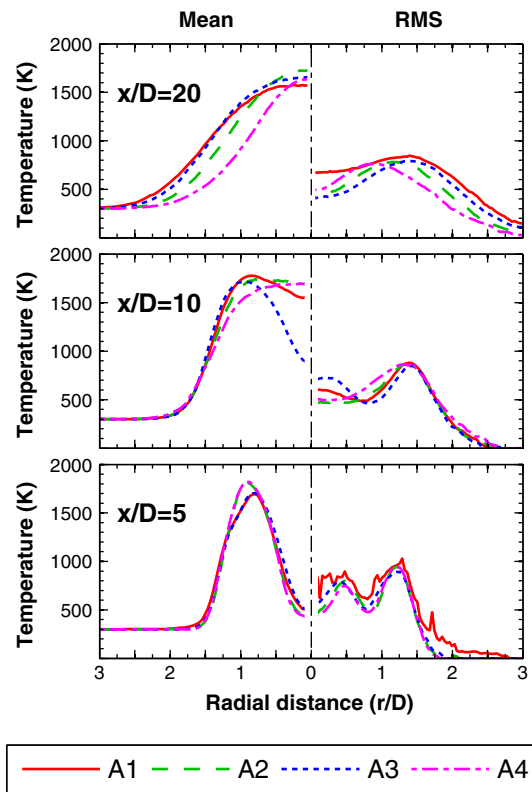

Fig. 7 Pseudo-unconditional temperature radial profiles (mean and root-mean-square) at various axial (x/D) locations for the four flames (refer to Table 1)

unambiguous measure that provides a useful approximation for the true mean. While the lower limit of 300 K seems unreasonable, it is chosen here as an extreme that separates the genuine NTLAF measurements from the remaining samples where no signal is detected. It is acknowledged that such samples will span the entire range from ambient to the NTLAF threshold, but there is no way of telling their relative abundance so selecting the extreme of 300 K is reasonable.

The trends of mean conditional temperature reported in Fig. 7 are consistent with expectations. Close to the jet exit plane $x/D = 5$, the peak mean temperature (of around 1,750 K) is similar in all flames since the pilot is dominant at this location. Further downstream, at $x/D = 20$, the largest temperature depression is for flame A4 which is closest to blow-off (refer to Table 1) followed by flame A2. Both in the shear layer on the lean side of the flame and near the jet centreline near the exit plane $x/D = 5$, the temperature RMS values are particularly high: a consequence of the high fluctuations between the points where temperature is available compared with the 300 K baseline value.

Consistent with the relatively uniform conditional temperature profiles noted in Fig. 6, it can also be observed

Fig. 8 Conditional temperature histograms for the four flames (refer to Table 1) at various axial (*x/D*) locations. The *red vertical dashed line* indicates the mean temperature for each flame at each *x/D* location
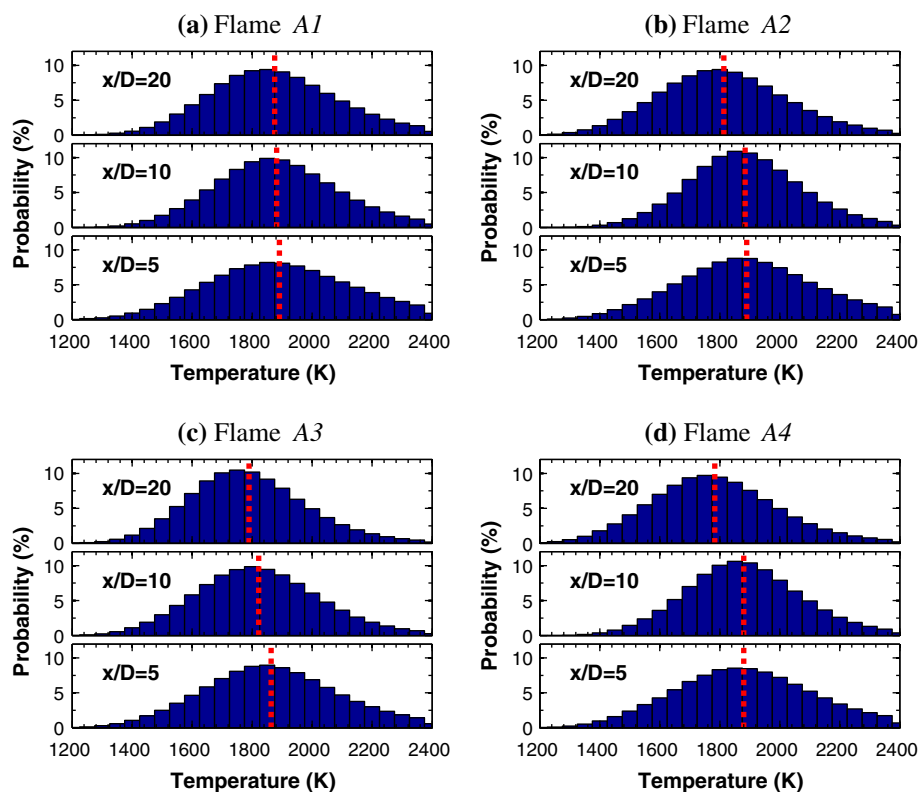

that the temperature histograms shown in Fig. 8 are also very similar in all flames and at all locations. Figure 8 provides further evidence that the evaporation process is occurring sufficiently far from the reaction zone to have little direct influence on the flame. Figure 8 shows that the mean temperature for each flame decreases with increasing *x/D*, as shown by the red vertical dashed lines. The reduction in the mean temperature with increasing *x/D* is most pronounced for the flames closest to blow-off (especially flame A4), and minor for the flames further from blow-off (especially flame A1).

The temperature histograms (Fig. 8) indicate that the lowest temperature for which data is collected is $\sim$1,200 K, and indeed, most are $\gtrsim$1,400 K. As mentioned in Sect. 3.3, the temperature threshold in the data processing is imposed to be 800 K. The scarcity of data between 800–1,200 K is attributed to a low concentration of indium at low temperatures due to the limited conversion of indium chloride to neutral indium atoms, compounded by low anti-Stokes population in that temperature range. Referring back to Fig. 5, it is apparent that in the potential core region, both the Stokes and anti-Stokes fluorescence signals are low. The lack of Stokes signal is indicative of a paucity of indium atoms in this region. A similar observation is noted at other locations such that, in general, a lack of anti-Stokes signal is also associated with a lack of Stokes signal. This indicates that

neutral indium atoms are simply not present below the 1,200 K temperature limit. This explains why the lower temperature limit for the anti-Stokes signal can be lowered to 800 K in these flames: in the 800–1,200 K range, the signal is below detection limits for both Stokes and anti-Stokes, and thus, the choice of the threshold does not affect the lower limit of the NTLAF technique for these spray flames.

Figure 9 presents mean temperature profiles comparing NTLAF with thermocouple measurements made with an *R*-type bead diameter of 0.5 mm (blue line with '+' symbols). Consistent with previous measurements (Stårner et al. 2005), no compensation is made for radiation or wet-bulb effects due to droplet interaction. It is estimated that in the worst case, these affects are approximately 100 K, but typically less. It should also be noted that the thermocouple measurements are used as a comparison with the NTLAF measurements and not as a validation. Each plot in Fig. 9 shows the NTLAF temperature mean calculated in two different ways. The black dotted line is the pseudo-unconditional mean described above. Conversely, the solid red line is the conditional mean. This is calculated from only the data points where the fluorescence is sufficiently high to give a meaningful temperature (although at the edges of the jet, it becomes more affected by noise). The conditional mean, therefore, does not account for cases where data are not available.

Fig. 9 Average NTLAF and thermocouple temperature measurements for the four flames at various x/D locations. The mean temperature from the NTLAF measurement is calculated using a pseudo-unconditional method and also conditional on indium fluorescence from both Stokes and anti-Stokes
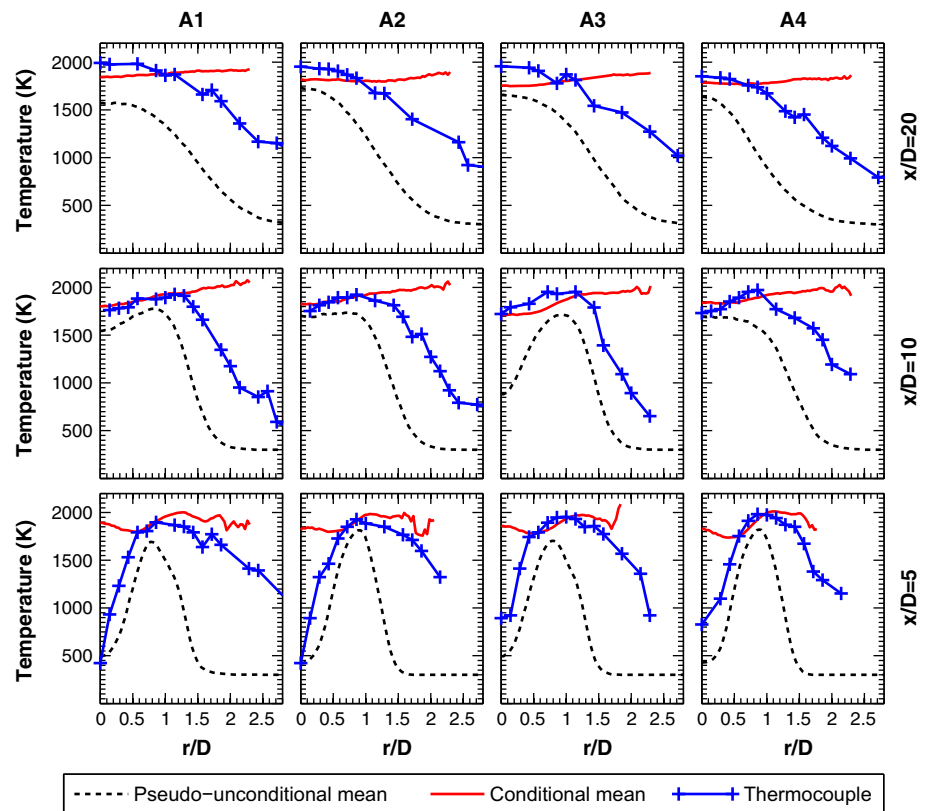
At $x/D = 5$, in the potential core of the flame where the signal is below detection limits, the mean NTLAF temperature measurements are biased (the unconditional mean is biased low, the conditional mean is biassed high). However, at outer radial locations closer to the reaction zone, all three temperature measurements converge to the same values, within experimental error. This gives confidence that the conditional temperature captures the reaction zone temperature reliably. The fact that the conditional mean and thermocouple measurements are remarkably similar at the peak indicates that NTLAF captures the correct temperature at the reaction zone. The pseudo-unconditional mean is understandably lower because of fluid pockets below the NTLAF threshold being set to 300 K. Further to the lean side, the unconditional mean becomes increasingly affected by the absence of data, but the conditional mean and thermocouple measurements are in reasonable agreement.

At $x/D = 10$, where the fluorescence intensity is greatest, the agreement between the measurements is best, except for a slight dip around $r/D \approx 0.5$ in flame A3. This is particularly true on the centreline where the mean temperatures are higher than at $x/D = 5$ indicating that droplets are not present in the reaction zone at this location. The agreement between the conditional mean and the thermocouple measurements is better than 100 K everywhere except on the fuel-lean side of the reaction zone, and this

compares favourably with previous comparisons of NTLAF against other thermometry approaches Medwell et al. (2013).

At $x/D = 20$, the thermocouple measurements are higher than the conditional mean NTLAF temperature. Importantly, considering that the conditional mean only includes data above the indium formation threshold of 1,200 K, it should be either equal to or higher than the mean measured with a thermocouple. This discrepancy is consistent with previous NTLAF measurements at locations approaching the tip of the flame (Medwell et al. 2013) and may point towards an unresolved systematic error in the NTLAF measurements in this region. Future comparisons with temperature measurements using CARS would be useful in resolving some of these issues.

4 Conclusions

Nonlinear excitation regime two-line atomic fluorescence (NTLAF) has been successfully applied to a set of turbulent dilute spray flames of acetone. The liquid fuel spray flames have, for the first time, been demonstrated to be highly effective for seeding indium required for NTLAF measurements. The detected fluorescence signal is found to be immune to scattering/interference from the spray droplets and vapour. No modifications to the

optical arrangement were required to transition from gaseous to spray flames. The dilute spray burner is well suited to NTLAF thermometry with potential for additional simultaneous measurements via other laser diagnostic techniques. These discoveries pave the way for future detailed experiments in turbulent dilute spray flames to develop understanding of this important class of spray flames.

Reliable NTLAF temperature measurements are reported in the reaction zone, and these trends are in excellent agreement with thermocouple measurements. There are limitations, however, in that the technique relies on the presence of neutral indium atoms in the measurement volume, and the conversion of indium chloride to neutral indium only initiates at around 1,200 K. Furthermore, indium oxidises on the lean side of the reaction zone.

References

Aldén M, Grafström P, Lundberg H, Svanberg S (1983) Spatially resolved temperature measurements in a flame using laser-excited two-line atomic fluoresence and diode-array detection. Opt Lett 8(5):241–243

Alkemade CTJ (1970) A theoretical discussion on some aspects of atomic fluorescence spectroscopy in flames. Pure Appl Chem 23(1):73–98

Bohlin A, Kliewer CJ (2013) Simultaneous planar imaging and multiplex spectroscopy in a single laser shot. J Chem Phys 138:221101

Bohlin A, Patterson BD, Kliewer CJ (2013) Simplified two-beam rotational CARS signal generation demonstrated. J Chem Phys 138:081102

Brackmann C, Bood J, Bengtsson PE, Seeger T, Schenk M, Leipertz A (2002) Simultaneous vibrational and pure rotational coherent anti-Stokes Raman spectroscopy for temperature and multispecies concentration measurements demonstrated in sooting flames. Appl Opt 41(3):564–572

Burns IS, Mercier X, Wartel W, Chrystie RSM, Hult J, Kaminski CF (2011) A method for performing high accuracy temperature measurements in low-pressure sooting flames using two-line atomic fluorescence. Proc Combust Inst 33:799–806

Chan QN, Medwell PR, Kalt PAM, Alwahabi ZT, Dally BB, Nathan GJ (2010) Solvent effects on two-line atomic fluorescence (TLAF) of indium. Appl Opt 49(8):1257–1266

Chan QN, Medwell PR, Kalt PAM, Alwahabi ZT, Dally BB, Nathan GJ (2011) Assessment of interferences to nonlinear two-line atomic fluorescence (ntlaf) in sooty flames. Proc Combust Inst 33:791–798

Chan QN, Medwell PR, Alwahabi ZT, Dally BB, Nathan GJ (2011) Assessment of interferences to nonlinear two-line atomic fluorescence (ntlaf) in sooty flames. Appl Phys B 104:189–198

Chan QN, Medwell PR, Dally BB, Alwahabi ZT, Nathan GJ (2012) New seeding methodology for gas concentration measurements. Appl Spectrosc 66(7):803–809

Dec JE, Keller JO (1986) High speed thermometry using two-line atomic fluorescence. Proc Combust Inst 21:1737–1745

Devillers R, Bruneaux G, Schulz C (2008) Development of a two line OH-laser-induced fluorescence thermometry diagnostics strategy for gas-phase temperature measurements in engines. Appl Opt 47(31):5871–5885

Engel SR, Koegler AF, Gao Y, Kilian D, Voigt M, Seeger T, Peukert W, Leipertz A (2012) Gas phase temperature measurements in the liquid and particle regime of a flame spray pyrolysis process using O₂ based pure rotational coherent anti-Stokes Raman scattering. Appl Opt 51(25):6063–6075

Engström J, Nygren J, Aldén M, Kaminski CF (2000) Two-line atomic fluorescence as a temperature probe for highly sooting flames. Opt Lett 25(19):1469–1471

Fansler TD, Drake MC, Gajdeczko B, Düwel I, Koban W, Zimmermann FP, Schulz C (2009) Quantitative liquid and vapor distribution measurements in evaporating fuel sprays using laser-induced exciplex fluorescence. Meas Sci Technol 20:125401

Gounder JD (2009) An experimental investigation of non-reacting and reacting spray jets. Ph.D. thesis, University of Sydney, Australia

Gounder JD, Kourmatzis A, Masri AR (2012) Turbulent piloted dilute spray flames: flow fields and droplet dynamics. Combust Flame 159:3372–3397

Haraguchi H, Smith B, Weeks S, Johnson DJ, Winefordner JD (1977) Measurement of small volume flame temperatures by the two-line atomic fluorescence method. Appl Spectrosc 31:156–163

Hult J, Burns IS, Kaminski CF (2005) Two-line atomic fluorescence flame thermometry using diode lasers. Proc Combust Inst 30:1535–1543

Jenny P, Roekaerts D, Beishuizen N (2012) Modeling of turbulent dilute spray combustion. Prog Energy Combust Sci 38:846–887

Kaminski CF, Engström J, Aldén M (1998) Quasi-instantaneous two dimensional temperature measurements in a spark ignition engine using 2-line atomic fluorescence. Proc Combust Inst 27:85–93

Kearney SP, Frederickson K, Grasser TW (2009) Dual-pump coherent anti-Stokes Raman scattering thermometry in a sooting turbulent pool fire. Proc Combust Inst 32:871–878

Köhler M, Geigle KP, Meier W, Crosland BM, Thomsom KA, Smallwood GJ (2011) Sooting turbulent jet flame: characterization and quantitative soot measurements. Appl Phys B 104:409–425

Kostka S, Roy S, Lakusta PJ, Meyer TR, Renfro MW, Gord JR, Branam R (2009) Comparison of line-peak and line-scanning excitation in two-color laser-induced-fluorescence thermometry of OH. Appl Opt 48(32):6332–6343

Kronemayer H, Bessler WG, Schulz C (2005) Gas-phase temperature imaging in spray systems using multi-line NO-LIF thermometry. Appl Phys B 81:1071–1074

Linne MA, Paciaroni M, Gord JR, Meyer TR (2005) Ballistic imaging of the liquid core for a steady jet in crossflow. Appl Opt 44(31):6627–6634

Linne MA, Paciaroni M, Berrocal E, Sedarsky D (2009) Ballistic imaging of liquid breakup processes in dense sprays. Proc Combust Inst 32:2147–2161

Linne M (2013) Imaging in the optically dense regions of a spray: a review of developing techniques. Prog Energy Combust Sci 39:403–440

Linne M, Sedarsky D, Meyer T, Gord J, Carter C (2010) Ballistic imaging in the near-field of an effervescent spray. Exp Fluids 49:911–923

MacPhee AG, Tate MW, Powell CF, Yue Y, Renzi MJ, Ercan A, Narayanan S, Fontes E, Walther J, Schaller J, Gruner SM, Wang J (2002) X-ray imaging of shock waves generated by high-pressure fuel sprays. Science 295:1261–1263

Masri AR, Gounder JD (2010) Turbulent spray flames of acetone and ethanol approaching extinction. Combust Sci Technol 182:702–715

Medwell PR, Chan QN, Kalt PAM, Alwahabi ZT, Dally BB, Nathan GJ (2009) Development of temperature imaging using two-line atomic fluorescence. Appl Opt 48(6):1237–1248

Medwell PR, Chan QN, Kalt PAM, Alwahabi ZT, Nathan GJ (2010) Instantaneous temperature imaging of diffusion flames using two-line atomic fluorescence. Appl Spectrosc 64(2):173–176

Medwell PR, Chan QN, Dally BB, Alwahabi ZT, Mahmoud S, Metha GF, Nathan GJ (2012) Flow seeding with elemental metal species via an optical method. Appl Phys B 107(3):665–668

Medwell PR, Chan QN, Dally BB, Mahmoud S, Alwahabi ZT, Nathan GJ (2013) Temperature measurements in turbulent nonpremixed flames by two-line atomic fluorescence. Proc Combust Inst 34:3619–3627

Nathan GJ, Kalt PAM, Alwahabi ZT, Dally BB, Medwell PR, Chan QN (2012) Recent advances in the measurement of strongly radiating, turbulent reacting flows. Prog Energy Combust Sci 38:41–61

Nygren J, Engström J, Walewski J, Kaminski CF, Aldén M (2001) Applications and evaluation of two-line atomic LIF thermometry in sooting combustion environments. Meas Sci Technol 12:1294–1303

O'Loughlin W, Masri AR (2011) A new burner for studying auto-ignition in turbulent dilute sprays. Combust Flame 158:1577–1590

O'Loughlin W, Masri AR (2012) The structure of the auto-ignition region of turbulent dilute methanol sprays issuing in a vitiated co-flow. Flow Turbul Combust 89:13–35

Omenetto N, Benetti P, Rossi G (1972) Flame temperature measurements by means of atomic fluorescence spectroscopy. Spectro-chim Acta 27B:453–461

Ramírez AI, Som S, Aggarwal SK, Kastengren AL, El-Hannouny EM, Longman DE, Powell CF (2009) Quantitative X-ray measurements of high-pressure fuel sprays from a production heavy duty diesel injector. Exp Fluids 47:119–134

Roy S, Gord JR, Patnaik AK (2010) Recent advances in coherent anti-Stokes Raman scattering spectroscopy: fundamental developments and applications in reacting flows. Prog Energy Combust Sci 36:280–306

Stårner SH, Gounder J, Masri AR (2005) Effects of turbulence and carrier fluid on simple turbulent spray jet flames. Combust Flame 143:420–432

Stelzner B, Hunger F, Voss S, Keller J, Hasse C, Trimis D (2013) Experimental and numerical study of rich inverse diffusion flame structure. Proc Combust Inst 34:1045–1055

Wang YJ, Im KS, Fezzaa K, Lee WK, Wang J, Micheli P, Laub C (2006) Quantitative x-ray phase-contrast imaging of air-assisted water sprays with high Weber numbers. Appl Phys Lett 89:151913

Weikl MC, Beyrau F, K. J., Seeger T, Leipertz A (2006) Combined coherent anti-Stokes Raman spectroscopy and linear Raman spectroscopy for simultaneous temperature and multiple species measurements. Opt Lett 31(12):1908–1910

Weikl MC, Seeger T, Wendler M, Sommer R, Beyrau F, Leipertz A (2009) Validation experiments for spatially resolved one dimensional emission spectroscopy temperature measurements by dual pump CARS in a sooting flame. Proc Combust Inst 32:745–752

Zizak G, Omenetto N, Winefordner JD (1984) Laser-excited atomic fluorescence techniques for temperature measurements in flames: a summary. Opt Eng 23(6):749–755